# Smectic-*A* structures in submicrometer cylindrical cavities

S. Kralj[1,2] and S. Žumer[2]
[1]*Department of Physics, Faculty of Education, University of Maribor, Koroška 160, 62000 Maribor, Slovenia*
[2]*Department of Physics, University of Ljubljana, Jadranska 19, 61000 Ljubljana, Slovenia*
(Received 13 November 1995; revised manuscript received 21 February 1996)

Model structures of a smectic-*A* liquid crystal confined to a long cylindrical cavity enforcing homeotropic surface anchoring are studied theoretically. The structures are obtained numerically through minimization of the Landau–de Gennes type free energy. We limit our discussion to cylinders with submicrometer radia. Five qualitatively different smectic-*A* configurations are proposed: the smectic-planar-radial, smectic-escaped-radial, chevron, bookshelf, and hybrid structures. Our analysis suggests that in the strong anchoring regime the smectic–escaped-radial structure is the most stable. For this structure relatively large temperature shifts of the nematic–smectic-*A* phase transition are expected. In the weak anchoring regime the chevron and bookshelf structures are found to be the most stable. We demonstrate that smectic elasticity can cause strong deviations from the preferred surface anchoring direction. [S1063-651X(96)07507-1]

PACS number(s): 61.30.Eb, 61.30.Jf, 61.30.Cz, 64.70.Md

## I. INTRODUCTION

Liquid crystals (LC) confined to curved geometries are currently attracting a lot of attention because of their potential use in electro-optic devices. In addition they exhibit a rich variety of physical phenomena that make them interesting from the fundamental point of view.

Most of the studies were performed on the confined nematic liquid crystals which are the simplest members of the LC family. So the behavior of a nematic liquid crystal in regular confining geometries (semi-infinite and finite slab geometry [1,2], spherical [3,4], and cylindrical [5–7] cavities) is relatively well understood. In the last few years several efforts have been made to understand behavior of nematic liquid crystals confined to cavities of irregular geometry [8] (e.g., porous glass matrices).

The next simplest LC phase is the smectic-*A* (Sm-*A*) phase [9]. In addition to the orientational ordering characteristic of the nematic phase it possesses also one dimensional positional order. In the simplest Sm-*A* phase molecules in parallel arrays of layers tend to be aligned along the layer normal. In confined samples the bulk Sm-*A* structure is deformed depending on the elastic properties, coupling to the external field, surface shape (roughness and curvature), surface coupling (yielding different kinds of anchoring, and wetting), and nematic history (the smectic layers tend to grow along the nematic director field).

There have been relatively few studies of the Sm-*A* phase constrained to curved geometry [10–15]. Most of them covered the Sm-*A* phase constrained to well defined cylindrical cavities (e.g., in glass capillaries [10,11], Nuclepore membranes [12,13], and Anopore membranes [14]) or solid matrices [15] with a random network of pores having locally cylinderlike shape. Unfortunately in most of these studies details of the structures of the confined Sm-*A* phase were not known.

The theories of the bulk Sm-*A* phase are rather well established [9,16]. They originate either from the molecular mean field or phenomenological macroscopic Landau-type description. The latter approach proved to be more adequate for our purpose. Most of the macroscopic phenomenological studies have been done in the framework of the harmonic approximation [17]. There, molecules are locked along the layer normal. For the description of the departures from this approximation the Landau-Ginsburg model is usually used [18–20]. This approach closely resembles [18,19] the theory developed to describe the transition to the superconducting phase in the metal.

In order to qualitatively explain recent experiments on the Sm-*A* phase constrained by curved geometries we decided to carry out a study of phenomenological description of Sm-*A* structures confined to a cylindrical environment. The paper is organized in the following way. Section II describes the free energy contributions. In Sec. III possible nematic director field structures are analyzed in the parent nematic phase. In Sec. IV different Sm-*A* layer structures are superimposed on these nematic profiles. The stability of structures is discussed and summarized in the last section.

## II. MODEL

To study different Sm-*A* structures confined to a long cylinder we use the Landau–de Gennes approach [9,18]. Structures are presented by the director field $\vec{n}(\vec{r})$, the nematic uniaxial orientational order parameter $S(\vec{r})$, and the smectic complex density wave $\tilde{\psi}(\vec{r})=\eta(\vec{r})e^{i\phi(\vec{r})}$. The positional order parameter $\eta$ describes a degree of layer ordering. The position of layers is defined by the phase factor $\phi$. We express the bulk free energy density $f(\vec{r})$ of our system as a sum of *local* and *nonlocal* contributions of nematic $(f_n^{\rm loc}, f_n^{\rm non})$ and smectic $(f_s^{\rm loc}, f_s^{\rm non})$ phase, and add a short range surface contribution $f_{\rm surf}$:

$$f=f_n^{\rm loc}+f_n^{\rm non}+f_s^{\rm loc}+f_s^{\rm non}+f_{\rm surf}\delta(\vec{r}-\vec{R}). \tag{1}$$

We retain only the minimum number of necessary terms in the free energy expansion and find the following well known forms [18–21]:

$$f_n^{\rm loc}=A(T-T^*)S^2-BS^3+CS^4, \tag{1a}$$

 

$$f_n^{\rm non}=\frac{K_{11}(\mathrm{div}\vec{n})^2}{2}+\frac{K_{22}(\vec{n}\cdot\mathrm{curl}\vec{n})^2}{2}+\frac{K_{33}(\vec{n}\times\mathrm{curl}\vec{n})^2}{2}+L(\mathrm{grad}S)^2, \tag{1b}$$

$$f_s^{\rm loc}=a(T-T_{NA})|\tilde{\psi}|^2+\frac{b|\tilde{\psi}|^4}{2}, \tag{1c}$$

$$f_s^{\rm non}=C_{\parallel}|(\vec{n}\cdot\mathrm{grad}-iq_0)\tilde{\psi}|^2+C_{\perp}|(\vec{n}\times\mathrm{grad})\tilde{\psi}|^2, \tag{1d}$$

$$f_{\rm surf}=W_0 g_{\rm surf}(\vec{n},\tilde{\psi}). \tag{1e}$$

Positive quantities $A,B,C,a,b$ are coefficients of the Landau–de Gennes expansion. They depend on the material properties of a liquid crystal and we assume that they are temperature independent. The supercooling temperature $T^*$ describes the lower limit of the existence of the isotropic phase. The first order isotropic-nematic phase transition takes place at the temperature $T=T_{NI}=T^*(B^2/4CA_0+1)>T^*$. The $N$–Sm-$A$ phase transition is realized at $T=T_{NA}$. In the model we consider only the case where this transition is continuous.

The elastic properties of the nematic phase are described by elastic constants $K_{11}$ (splay), $K_{22}$ (twist), $K_{33}$ (bend), and $L$ where [21] $K_{ii}\propto S^2+$higher order terms ($ii=11,22,33$). The smectic elasticity is controlled by the smectic bend ($C_{\perp}$) and compressibility ($C_{\parallel}$) elastic constant [19]. As we are looking for a qualitative picture this description of the system is by no means complete. We have, e.g., not taken into account the ''surface'' nematic elastic constants [22] $K_{24}$,$K_{13}$. For a more complete description of the nematic components see Refs. [6, 21]. The adequacy of the contribution to the free energy describing the smectic component is discussed in detail [16] by Linhananta and Sullivan.

The surface contribution $f_{\rm surf}$ [Eq. (1e)] is modeled with the $\delta$ function with the strength of the surface coupling $W_0$. The dimensionless function $g_{\rm surf}$ describes the details of the coupling between the LC order parameters and the surface. In our discussion only the nematic orientational anchoring is taken into account. This term is conventionally expressed as [1,23]

$$g_{\rm surf}=-\frac{S}{2}(\vec{n}\cdot\vec{e}_{\rm easy})^2. \tag{2}$$

Here the vector $\vec{e}_{\rm easy}$ describes the easy axis imposed by the surface (i.e., for the homeotropic anchoring $\vec{e}_{\rm easy}$ points along the surface normal).

In the following we simplify Eq. (1) and rewrite it into the dimensionless form which is adequate for computational reasons. We introduce ''bare'' nematic elastic constants $k_{ii}=K_{ii}/S^2$ ($ii=11,22,33$) and bulk order parameters $S_b=S(T=T_{NI})=B/(2C)$, $\eta_b(T=0)=aT_{NA}/b$. Here $S_b$ describes degree of nematic ordering at the $N$-$I$ transition and $\eta_b$ estimates the saturated degree of translational ordering deep in the Sm-$A$ phase of the unconstrained LC. We simplify the problem by adopting the following approximations: (i) $k_{ii}$ are temperature independent, (ii) $k_{11}=k_{22}=k_{33}=L\equiv k$, and (iii) $C_{\parallel}=C_{\perp}$.

In order to express $f(\vec{r})$ with the smallest set of experimentally measurable quantities we introduce some temperature independent characteristic lengths [9,24]. These are the smectic zero temperature coherence length $\xi_s=\sqrt{C_{\parallel}/(aT_{NA})}$, the nematic zero temperature coherence length $\xi_n=\sqrt{k/(AT_{NI})}$, the nematic penetration length $\lambda=\sqrt{S_b^2k/(\eta_b^2C_{\parallel}q_0^2)}$, and the surface extrapolation length $d_e=kS_b^2/W_0$. Values of $d_e$ typically extend from a nm (strong anchoring) to a $\mu$m regime (weak anchoring). For a typical LC material the quantities $\xi_s$, $\xi_n$, and $\lambda$ are comparable to the length of LC molecules. They are related to temperature dependent lengths describing characteristic scales on which the system responds to various perturbations. Within our phenomenological description in the temperature regime $T<T_{NA}$ one can approximately write [9,24]

$$\xi_s(T)\approx\xi_s\left(\frac{T_{NA}}{T_{NA}-T}\right)^{1/2},\quad \xi_n(T)\approx\xi_n\left(\frac{T_{NI}}{T^*-T}\right)^{1/2},\quad \lambda(T)\approx\lambda\left(\frac{T_{NA}}{T_{NA}-T}\right)^{1/2}. \tag{3}$$

Thus for the second order $N$–Sm-$A$ transition $\xi_s(T)$ and $\lambda(T)$ diverge at $T=T_{NA}$.

We further introduce dimensionless operators $\vec{\nabla}\equiv R\,\mathrm{grad}$, $\vec{\nabla}\times\equiv R\,\mathrm{curl}$, $\vec{\nabla}\cdot\equiv R\,\mathrm{div}$, and dimensionless cylindrical coordinates $(\rho,\varphi,z)$. Coordinates $\rho$ and $z$ are measured in units of the cylinder radius $R$. Thus the cylinder wall is at $\rho=1$. Unit vectors along cylindrical coordinates are designated by $\vec{e}_\rho,\vec{e}_\varphi,\vec{e}_z$. We define the scaled nematic $q=S/S_b$, and smectic order parameter $\epsilon=\eta/\eta_b$, scaled density wave $\psi=\tilde{\psi}/\eta_b=\epsilon e^{i\phi}$, dimensionless temperature $t=T/T_{NI}$, ratios $t_A=T_{NA}/T_{NI}$, $t_*=T^*/T_{NI}$, and dimensionless characteristic inverse lengths $r_q=q_0R$, $A_s=R/\xi_s$, $A_n=R/\xi_n$, $A_\lambda=R/\lambda$, and $A_{\rm surf}=R/d_e$ measured in units of $R$. On this reduced temperature scale the bulk $N$-$I$ transition takes place at $t=1$, where $q$ jumps from $q=0$ to 1. The nematic supercooling limit corresponds to $t=0$. The introduced bulk order parameters $S_b=S(T=T_{NI})$, $\eta_b=\eta(T=0)$ correspond to $q(t=1)=1$ and $\epsilon(t=0)=1$, respectively. The dimensionless free energy density $g$ can be expressed as

$$g=f/(C_{\parallel}\eta_b^2/R^2)=A_s^2g_s^{\rm loc}+g_s^{\rm non}+\left(\frac{r_q}{A_\lambda}\right)^2\left[A_n^2(g_n^{\rm loc}+g_n^{\rm non})+A_{\rm surf}+g_{\rm surf}\delta\left(\frac{\vec{r}}{R}-\vec{e}_{\rm easy}\right)\right] \tag{4}$$

where

$$g_n^{\rm loc}=(1-t_*)\left(\frac{t-t_*}{1-t_*}q^2-2q^3+q^4\right), \tag{4a}$$

$$g_n^{\rm non}=q^2\left(\frac{(\vec{\nabla}\cdot\vec{n})^2}{2}+\frac{(\vec{\nabla}\times\vec{n})^2}{2}\right)+(\vec{\nabla}q)^2, \tag{4b}$$

$$g_s^{\rm loc}=\frac{t-t_A}{t_A}\epsilon^2+\frac{\epsilon^4}{2}, \tag{4c}$$

$$g_s^{\rm non}=\epsilon^2(\vec{n}\cdot\vec{\nabla}\phi-r_q)^2+(\vec{n}\cdot\vec{\nabla}\epsilon)^2+\epsilon^2(\vec{n}\times\vec{\nabla}\phi)^2 + (\vec{n}\times\vec{\nabla}\epsilon)^2, \tag{4d}$$

$$g_{\rm surf}=-\frac{q}{2}\,(\vec{n}\cdot\vec{e}_{\rm easy})^2\,. \tag{4e}$$

In the following we discuss various Sm-*A* structures that can be realized within the cylinder whose surface enforces homeotropic anchoring.

## III. STRUCTURES—NEMATIC PHASE

Let us assume that the Sm-*A* phase is reached on cooling from the *N* phase. The smectic layer pattern within the cylinder is in this case strongly influenced by the nematic director orientation at the *N*–Sm-*A* transition. Therefore we first examine possible nematic structures and then superimpose smectic layers on nematic director profiles. We do not cover cases with smectic edge dislocations.

The stability of nematic structures in a cylindrical cavity with homeotropic surface anchoring has been studied in detail in Refs. [5, 6]. For the strong homeotropic anchoring the escaped-radial (ER) structure [5] is the most common situation. The director field perpendicular to the surface at the cylinder wall approaching the cylinder center gradually reorients until it points along the symmetry axis at $\rho=0$. If the surface anchoring strength is decreased, $\vec{n}(\rho=1)$ can deviate from the $\vec{e}_\rho$ direction, increasing its $z$ component. This happens in the regime [6] $R/d_e<10$. With decreasing $R/d_e$ the director field gradually transforms into the homogeneous ($H$) structure in which the director field everywhere points along the cylinder axis. For $K_{24}=K_{13}=0$ this happens [5,6] at $R/d_e=(R/d_e)_{\rm crit}=2$.

In some cavities, instead of the ER structure, the escaped-radial structure with point defects stabilized either by imperfections in the cylinder or by effects at the ends of the cavity [5]. The domains with the escaped-radial pattern are separated by planes where the director field is completely radial. Along the symmetry axis of such planar director fields there are alternatively radial and hyperbolic point defects [25].

Approaching the Sm-*A* phase by decreasing the temperature, the smectic fluctuations yield an increase [9] of bend and twist elastic nematic constants. For a continuous transition these constants diverge at $T_{NA}$. As a consequence the ER structure becomes less stable than the planar-radial (PR) structure [5] with pure splay. In this structure the director field points everywhere radially towards the line defect of strength 1 along the cylinder axis.

## IV. STRUCTURES—Sm-*A* PHASE

Based on the ''nematic'' history we propose five qualitatively different smectic structures which are allowed from the topological point of view. According to their appearance we name them (a) the smectic-planar-radial (SPR), (b) the smectic-escaped-radial (SER), (c) the chevron (CHV), (d) the bookshelf (BKS), and (e) the hybrid (HBR) structure. They are schematically presented in Figs. 1(a)–1(e). The SPR structure is superimposed on the planar-radial director profile, SER, CHV, HBR on the escaped-radial field, and BKS on the escaped-radial or homogeneous nematic pattern. In the following we briefly summarize their main characteristics for the (i) strong and (ii) weak surface anchoring.

We first introduce adequate parametrization for $\vec{n}(\vec{r})$ and $\phi(\vec{r})$ that are used in numerical calculations. The nematic director field of all the structures is described by $\vec{n}=\vec{e}_\rho\sin\theta+\vec{e}_z\cos\theta$, $\theta=\theta(\rho)$. In the SPR structure $\theta(\rho)=\pi/2$, everywhere. This parametrization excludes structures with the twist nematic distortions. The phase factor of the SER and SPR structures is parametrized as $\phi(\vec{r})=r_q\rho$. For the chevron and bookshelf structures we use [20] $\phi(\vec{r})=r_q\nu z+u(\rho)$, where $\nu$ is the variational parameter. The BKS structure is established for $\nu=1$. If $\nu<1$ the CHV profile is realized instead, with layer normal along the vector $(\sin\theta_{\rm CHV},0,\cos\theta_{\rm CHV})$, where $\nu=\cos\theta_{\rm CHV}$. The quantity $u(\rho)$ describes displacement of smectic layers in the $z$ direction. In the harmonic approximation, where $\vec{n}$ is constrained along the smectic normal, one can use [20] $du/d\rho=\nu r_q\tan\theta$. The describe the hybrid structure we use parametrization $\phi(\vec{r})=r_q\rho$ for $\rho>\rho_c>0$ and $\phi(\vec{r})=r_q\nu z+u(\rho)$ for $\rho<\rho_c<1$.

Euler-Lagrange equations determining continuum fields $u(\rho)$, $\phi(\rho)$, $\epsilon(\rho)$, and $q(\rho)$ are obtained via minimization of the free energy functional. Calculated spatial dependencies of the director field and order parameters are shown in Figs. 2–4. The corresponding layer structures are schematically presented in Figs. 1(a)–1(e). All the structures are evaluated for the case of smooth surface. The material parameters entering Eqs. (4) are set to

$$A_s^2=10\,000,\quad A_n^2(1-t_*)=100,\quad t_A=1,\quad t_*=0.997,\quad r_q=100,\quad A_\lambda=100. \tag{5}$$

The choice simulates a typical liquid crystal [9] (5CB) in a cavity of radius $R=0.1$ $\mu$m which has been used in most recent experiments [12–14].

### A. Strong homeotropic anchoring

*First* we consider cases where the surface is smooth on the scale of the smectic correlation length and enforces strong homeotropic anchoring.

In the smectic planar-radial structure [Fig. 1(a)] the director profile is radial and the Sm-*A* layers are stacked in the $\vec{e}_\rho$ direction. Along the axis of the cylinder the liquid crystal has a paranematic (weakly ordered nematic) core. The corresponding $q(\rho)$ and $\epsilon(\rho)$ spatial dependencies are shown in Fig. 2(a). The defect in the director field at $\rho=0$ enforces $q(0)=0$. But despite the singularity in the nematic component the smectic part of the free energy density is not singular at the cylinder axis. Therefore within the model a finite value of $\epsilon(0)$ is allowed although this region is isotropic. We believe that this weak point of the model can be cured by taking into account coupling between the smectic and the nematic order parameter. The way in which $q$ and $\epsilon$ are coupled is still questionable. de Gennes and Prost [9] proposed term $q\epsilon^2$. According to molecular mean field theory [16] developed by Linhananta and Sullivan this coupling is more complicated. The straightforward possibility is to include higher order coupling terms [19] in the free energy, e.g., $\propto|(\vec{n}\times\vec{\nabla})^2\tilde{\psi}|^2$. This term is proportional to second de-

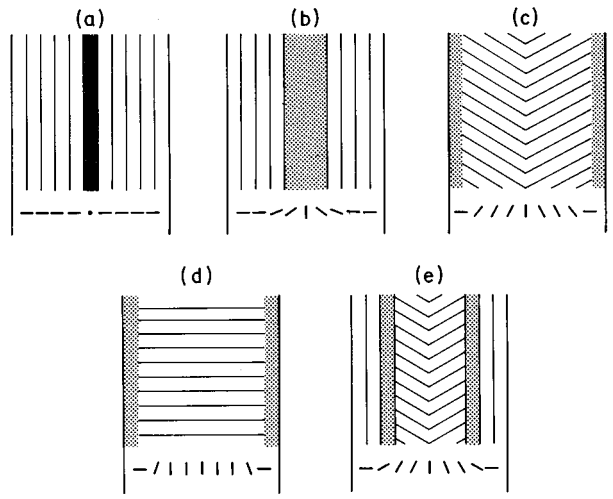


FIG. 1. Schematic presentation of different Sm-*A* structures for the case of strong homeotropic anchoring and smooth surface: (a) SPR, (b) SER, (c) CHV, (d) BKS, and (e) HBR structure. The smectic layers are drawn with the full line. The nematic director field spatial variation is indicated at the bottom part of each structure. The dotted regions describe places where nematic (a) or smectic (a)–(e) ordering melts.

rivatives of $\psi$ that resist the bending of smectic layers, unlike smectic terms given in Eq. (1d). In accordance with this picture we calculated the corrected SPR profiles enforcing $\epsilon(0)=0$. In addition this is also the simplest way to remove the compressibility problem arising in small cylinders if the radius is not commensurate with the layer thickness [26].

For the case of strong anchoring the escaped-radial director profile cannot coexist with the Sm-*A* layering in the whole cylinder because of the antagonistic boundary conditions $\vec{n}(\rho=0)=\vec{e}_z$ and $\vec{n}(\rho=1)=\vec{e}_\rho$. In order to resolve this problem without dislocations the Sm-*A* phase locally melts either (i) in the center, (ii) at the surface of the cylinder, or (iii) somewhere in between. These scenarios correspond to the (i) SER, (ii) CHV, BKS, and (iii) HBR structure, respectively. The spatial profile of structures based on the escaped-radial director profile is shown in Figs. 2(b)–2(e) deep in the Sm-*A* phase. The plot $q(\rho)$ is not shown because local nematic elastic distortions are not strong enough to cause substantial local depression of the orientational order parameter.

In the smectic escaped-radial structure [Figs. 1(b), 2(b)] the smectic layers are stacked in the radial direction. On approaching $\rho=0$ the director field tends to persist in the $\vec{e}_\rho$ direction [$\theta(\rho)\approx\pi/2$] to minimize the Sm-*A* elastic free energy penalty. Near the symmetry axis of the cylinder it gradually reorients along the $z$ coordinate [$\theta(1)=0$] in order to avoid defect in the nematic component. Accompanying strong bend deformation melts smectic layers in this region.

In the chevron structure [Figs. 1(c), 2(c)] the smectic layers run along the $z$ axis and adopt the chevron profile. The nematic component exhibits relatively large bend distortions at $\rho=0$ and 1, which causes local smectic melting. Note that the chevron profile shown is not minimized through $\theta_{\mathrm{CHV}}$, which was enforced by setting $\theta_{\mathrm{CHV}}=\pi/4\neq\theta(1)=\pi/2$. If $\theta_{\mathrm{CHV}}$ is treated as the variational parameter it tends to approach a value of $\theta(1)$. Thus in the case of strong anchoring $\theta_{\mathrm{CHV}}=\pi/2$ and the CHV structure is identical to the SER profile.

In the bookshelf structure [Figs. 1(d), 2(d)] the layer normal points along the cylinder axis. To achieve this the director profile abruptly reorients from the $\vec{e}_\rho$ direction at the surface along $\vec{e}_z$ on the distance given by the smectic penetration length. This causes melting of Sm-*A* layers at the surface and the appearance of a highly bent nematic layer. Numerical calculations show that this structure is always substantially more energetic than its ''direct competitive'' CHV structure.

In the hybrid structure [Fig. 4(e)] the smectic layers are stacked in the $\vec{e}_\rho$ direction in the region $\rho\geqslant\rho_c$, where $\theta(\rho)\approx\pi/2$. At $\rho=\rho_c$ the ER director pattern exhibits large enough bend distortion of the director field to cause melting of smectic layers. In the region $\rho<\rho_c$ the smectic order recovers and layers run along $\vec{e}_z$. In order to minimize the smectic distortion layers adopt a chevron structure. In Fig. 1(e) the case is shown where $\theta_{\mathrm{CHV}}\approx\pi/3$, $\rho_c\approx0.6$. This choice reproduces the deuterium NMR results obtained by Crawford *et al.* [13]. Note that this set of parameters does not correspond to the configuration minimizing the free energy of our model. If $\theta_{\mathrm{CHV}}$ and $\rho_c$ are treated as variational parameters the pattern tends to evolve into the SER structure. But we have to bear in mind that in general confined liquid crystals often exhibit hysteresis [5,6]. Structures obtained in cavities often do not correspond to the global minimum of the free energy. They are caught in metastable states reflecting the history of a sample. As we could not find any other nematic director and smectic profile which can even qualitatively reproduce experimental results given in Ref. [13] we believe that our picture is at least qualitatively correct.

#### *1. Stability of structures*

We now analyze the stability of these structures. From the discussion above it follows that in the strong anchoring case either the SPR, SER, or HBR structure is possible. For the given condition and $t=0.97$ the corresponding scaled free energies $G_i=\int_0^1 g_i\rho\,d\rho$ ($i$=SPR, SER, hbr) are $G_{\mathrm{SPR}}\approx26.2$, $G_{\mathrm{SER}}\approx2.7$, $G_{\mathrm{HBR}}\approx4.0$, revealing stability of the SER structure. The situation does not change much for a different choice of parameters deep in the Sm-*A* phase close to the reference set given in Eq. (5). Thus at least within this model the stability of the SPR structure is very unlikely.

Further we have to discuss the effect of nematic bend and twist elastic constants in the Sm-*A* phase. On approaching the Sm-*A* phase from the *N* phase, $K_{22}$ and $K_{33}$ exhibit anomalous increase because of Sm-*A* fluctuations. So-called cybotatic [9] clusters with the Sm-*A* ordering form resisting to bend and twist elastic deformations. In the Sm-*A* phase the smectic elastic constants took over this role. For this reason we chose for nematic elastic constants deep in the Sm-*A* phase the same values as in the nematic phase far above $T_{NA}$. This is justified only if the Sm-*A* ordering is substantial across the whole sample. The regions, where the Sm-*A* phase is locally melted, correspond to an effective increase in the temperature above $T_{NA}$. Consequently we believe that in these melted regions anomalously increased bend and twist elastic constant should be taken into account. This would

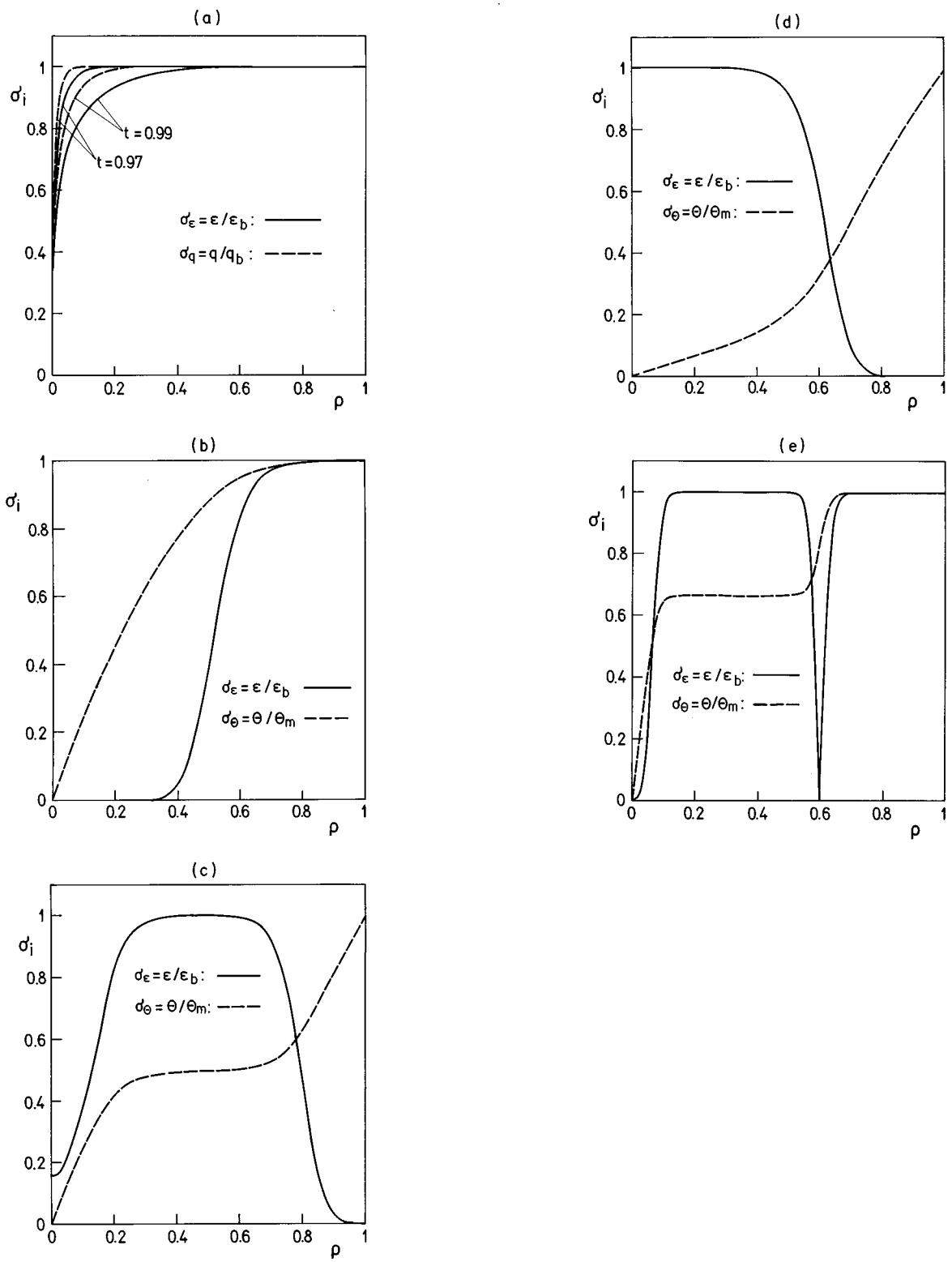


FIG. 2. Scaled parameters $\sigma_i$ versus $\rho(\sigma_\epsilon=\epsilon/\epsilon_b$, $\sigma_\theta=\theta/\theta_m$, $\sigma_q=q/q_b)$ for different Sm-$A$ structures for strong homeotropic anchoring. The SPR structure (a) is plotted at $t=0.97$ and 0.99 (corresponding to $T=290$ and 299 K for $T_{NA}\approx T_{NI}=300$ K). The SER (b), CHV (c), BKS (d), and HBR (e) structures are calculated at $t=0.97$. Values of material parameters are equal to the reference set (5) with exception $A_s=r_q=300$ in (e). $\epsilon_b$, $q_b$ are the bulk values of order parameters and $\theta_m=\theta(1)=\pi/2$.

result in narrower regions where nematic bend elastic deformation is strong. See Fig. 3, which illustrates the case of the SER structure. With increasing $K_{33}/K_{11}$ ratio the central melted region decreases. Consequently the SER structure becomes more distorted in the nematic component approaching the SPR profile. Thus the free energies of these structures become comparable if smectic fluctuations in the melted region are taken into account.

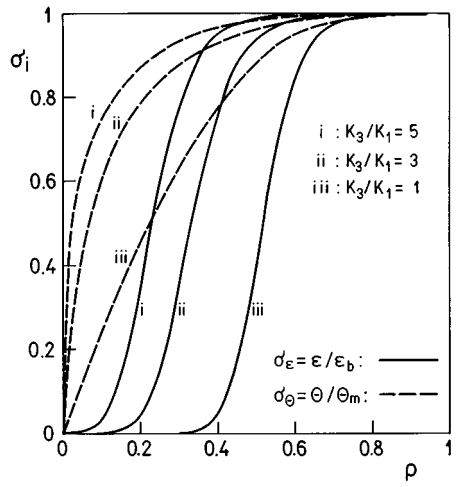


FIG. 3. The SER structure for different ratios of $K_{33}/K_{11}$: (i) $K_{33}/K_{11}=1$, (ii) $K_{33}/K_{11}=3$; (iii) $K_{33}/K_{11}=5$. $t=0.97$ and values of other material constants are given in (5).

### *2. Temperature shift of phase transitions*

In the SPR structure the elastic smectic distortions are rather weak. Assuming $\epsilon(\rho)=\epsilon_b$ $g_s^{\rm non}=0$ holds. Here $\epsilon_b$ stands for the bulk value minimizing $g_s^{\rm loc}$. Consequently we do not expect a large $N$–Sm-$A$ transition temperature shift $\Delta T_{NA}=T_{NA}-T_{NA}(R)>0$ induced by the confinement.

In contrast the escaped radial nematic profile in the strong anchoring regime relatively hardly accommodates the layered Sm-$A$ structure. As a consequence the temperature shift $\Delta T_{NA}$ of the onset of the Sm-$A$ phase with the SER, CHV, BKS, or HBR smectic structure is expected to be relatively large. To estimate $\Delta T_{NA}$ we consider a simplified case where (i) the ER profile is the same as in the nematic phase, (ii) $\epsilon=\epsilon_b$, and (iii) smectic layers run undistorted along the $z$ axis or radially. For these cases [5] $\theta(\rho)=2\tan^{-1}\rho$ holds. Thus for the layers along the $z$ axis $g_s^{\rm non}=2r_q^2\epsilon_b^2(1-\cos\theta)$ and the transition temperature shift is

$$\frac{\Delta T_{NA}}{T_{NA}}=\frac{4r_q^2}{A_s^2}\,\frac{\pi-3}{2}. \tag{6a}$$

Correspondingly for the layers along the radial direction $g_s^{\rm non}=2r_q^2\epsilon_b^2(1-\sin\theta)$ with the transition temperature shift

$$\frac{\Delta T_{NA}}{T_{NA}}=\frac{4r_q^2}{A_s^2}\,(1-\ln 2). \tag{6b}$$

The estimated temperature shifts are for conventional LC extremely large ($\Delta T$ is comparable to $T_{NA}$).

This indicates that for strong anchoring the transition temperature $T_{NA}(R)$ of the Sm-$A$ phase exhibiting the SER, CHV, BKS, or HBR smectic pattern is in general substantially shifted below $T_{NA}$, although in an actual situation the temperature shift would certainly be reduced because the director profile can adjust itself to Sm-$A$ layers departing from the ''conventional'' ER director profile.

Numerical calculations support this expectation. We find the smectic structures based on the escaped-radial nematic profile only at relatively low temperatures. For smaller ratio $r_q/A_s$ the temperature shift $\Delta T_{NA}$ is lower in qualitative accordance with Eqs. (6).

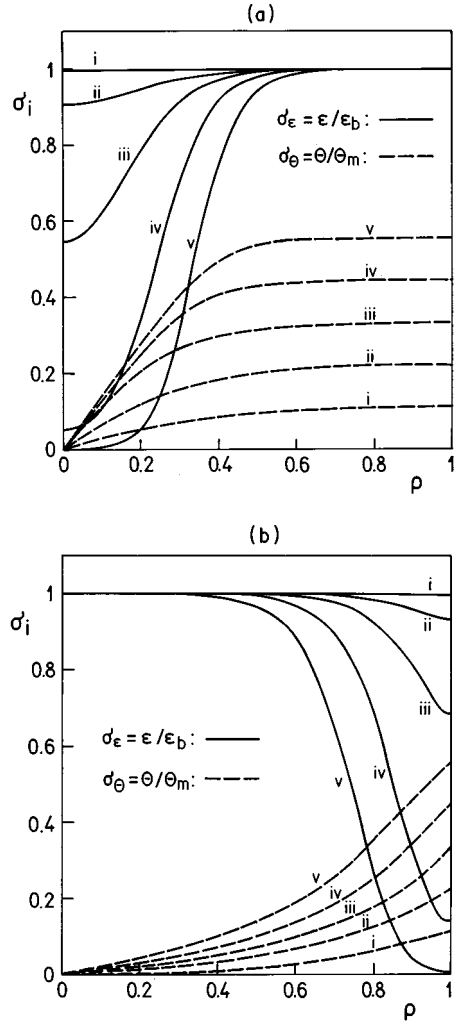


FIG. 4. The CHV (a) and BKS (b) structures in the weak anchoring regime. Spatial dependencies of scaled parameters $\sigma_i$ ($\sigma_\epsilon=\epsilon/\epsilon_b$, $\sigma_\theta=\theta/\theta_m$) are shown for the cases (i) $\theta(1)=0.1\theta_m$, (ii) $\theta(1)=0.2\theta_m$, (iii) $\theta(1)=0.3\theta_m$, (iv) $\theta(1)=0.4\theta_m$, (v) $\theta(1)=0.5\theta_m$; $\theta_m=\pi/2$ and $\epsilon_b$ denotes the bulk value of $\epsilon$. $t=0.97$ and values of other parameters are given in the reference set (5).

### B. Weak homeotropic anchoring

If the surface orientational anchoring is weak, substantial deviations of $\vec{n}(\rho=1)$ from the $\vec{e}_\rho$ direction occur and the ER director field is much less deformed than in previous cases. The appearance of the chevron or bookshelf structures is expected. The Sm-$A$ phase can now coexist with the ER profile in the whole cylinder, thus $\epsilon(\rho)\approx\epsilon_b$. Consequently also the transition temperature depression $\Delta T_{NA}$ is smaller. Corresponding director profiles are shown in Figs. 4(a) and 4(b) for different values of $\theta(1)$.

In the CHV structure we assume that the chevron profile is induced by the tilted nematic director at the surface, i.e., $\theta_{\rm CHV}=\theta(\rho=1)$. In this case the smectic elastic distortions are present in the region close to the axis of the cylinder. In contrast in the BKS structure both smectic and nematic dis-

tortions are localized in a region close to the surface. From Fig. 4 it is evident that in both structures the local melting is pronounced if $\theta(1)>\pi/4$. The CHV structure has substantially lower smectic elastic penalties because the elastic deformations are constrained to relatively smaller volume. As a consequence $G_{\mathrm{CHV}}<G_{\mathrm{BKS}}$, which indicates that the BKS structure can be stable only in a very weak anchoring regime where $\theta(1)\approx 0$ and the BKS and CHV structure are practically indistinguishable.

One should remember that the presented structures (Fig. 4) were evaluated enforcing a fixed value $\theta(1)$ at the surface with the implicit assumption that the resulting structures mimic the cases of certain weak anchoring strengths. The resulting dependence $\theta(\rho)$ is certainly not exactly equivalent to that obtained from the complete minimization procedure, where also $\theta(1)$ results from the minimization. Our approximation is justified by numerical results for the chv structure which reveal that the difference between these two approaches for the same value of $\theta(1)$ are negligible.

#### *1. Influence of the Sm-A elasticity on the surface angle*

In the weak anchoring regime the surface angle $\theta(1)$ is influenced by the presence of the smectic phase. In the *N* phase the balance between the nematic elastic forces and the surface anchoring enforces [5] $\theta(\rho=1)=\cos^{-1}[1/(A_{\mathrm{surf}}-1)]$ for the ER director profile. This expression corresponds to equal Frank elastic constants [9] and $K_{24}=0$. The value of $\theta(1)$ drops to zero at $A_{\mathrm{surf}}=A_{\mathrm{crit}}\equiv 2$ where a continuous transition [5,6] from the ER to the *H* nematic profile occurs.

In order to estimate the effect of the smectic ordering on $\theta(1)$ we assume that spatial variations in $\epsilon$ and $q$ are negligible. To simplify calculations we set $\epsilon=\epsilon_b$, $q=q_b=1$. In this regime $\theta(\rho)\ll 1$, thus the nonlocal part of $g_{\mathrm{BKS}}$ including surface contribution can be approximately expressed as

$$g_{\mathrm{BKS}}^{\mathrm{non}}+g_{\mathrm{surf}}\approx \epsilon_b^2 r_q^2\frac{\theta^4}{2}+\left(\frac{r_q}{A_\lambda}\right)^2\left\{\left[\frac{1}{2}\left(\frac{\partial\theta}{\partial\rho}\right)^2+\frac{1}{\rho}\left(\frac{\partial\theta}{\partial\rho}\right)\times\left(\theta-\frac{2\theta^3}{3}\right)+\frac{1}{2\rho^2}\left(\theta^2\frac{\theta^4}{3}\right)\right]+\frac{A_{\mathrm{surf}}}{2}\times\left(1-\theta^2+\frac{\theta^4}{3}\right)\delta(\rho-1)\right\}. \tag{7}$$

We further assume that $\theta\approx\theta_0\rho$, where $\theta_0$ is a constant. This approximation, which is for $\theta(1)<1$ in accordance with numerical results, enables us to evaluate $G(\theta_0)=\int_0(g_{\mathrm{BKS}}^{(\mathrm{non})}+g_{\mathrm{surf}})\rho\,d\rho$. Minimization of $G(\theta_0)$ with respect to $\theta_0$ yields an equation for $\theta_0$. The amplitude $\theta_0$ is different from zero only if $A_{\mathrm{surf}}>A_{\mathrm{crit}}\equiv 2$. Thus the threshold for the onset of the escaped radial structure is the same as in the *N* phase. The amplitude evolves with increasing anchoring strength as

$$\theta_0=\theta(1)\approx\left(\frac{6(A_{\mathrm{surf}}-A_{\mathrm{crit}})}{4A_{\mathrm{surf}}-5+2\epsilon_b^2A_\lambda^2}\right)^{1/2}. \tag{8}$$

If the cavity is large compared to $\lambda\approx a_0$, where $a_0$ describes typical molecular size, then $A_\lambda=R/\lambda\gg 1$. Consequently $\theta(1)\approx\sqrt{3(A_{\mathrm{surf}}-A_{\mathrm{crit}})/\epsilon_b^2A_\lambda^2}$. From this estimate it follows that the smectic component strongly influences the director angle on the surface $\theta(1)$. Its evolution with the increasing anchoring strength is much slower than in the *N* phase.

### C. Tangential anchoring

Although we are discussing the homeotropic anchoring situation it is worthwhile to mention that the CHV or the BKS structure can also be realized in the case of tangential anchoring. For the isotropic tangential anchoring and smooth surface the Sm-*A* structure with lowest energy corresponds to undistorted smectic layers running along the *z* direction characteristic for the BKS structure. The CHV profile is established if the surface enforces translational periodicity which is larger than the layer period in the bulk Sm-*A* phase [20].

### D. Rough surface

For rough surfaces it was proven [27] that the smectic and in some cases also the nematic phase is ''melted.'' So one can say that the surface is wetted by a nematic or isotropic phase. Therefore in the case of rough surfaces the effective anchoring strength is substantially reduced.

## V. CONCLUSIONS

We analyzed possible Sm-*A* structures in a long cylinder with homeotropic surface anchoring using the phenomenological Landau–de Gennes type description. Our attention was focused to cylindrical cavities of submicrometer radius. The approximation of equal smectic and nematic elastic constants was used. In particular we studied the influence of the orientational anchoring. The cases with dislocations in the smectic layer structure were not treated. The main purpose of our study is to clarify Sm-*A* structures in recent experimental studies [11–14]. We believe that the approximations used in our problem which grossly simplify the mathematics do not cause qualitative deviations from the reality.

In the strong anchoring regime deep in the Sm-*A* phase the smectic-escaped-radial structure is expected to occur while the chevron or bookshelf structure are expected to dominate in the weak anchoring regime. In these structures smectic layers are superimposed on the escaped-radial or homogeneous nematic director profile. In the SER structure the smectic layers are stacked radially from the surface. Strong smectic elastic distortions are constrained to the interior of the cylinder causing local melting of the layers. In the weak anchoring regime the CHV or BKS structures are realized. In both structures the layers are stacked along the cylinder axis. In the CHV structure the layers adopt the chevron profile. This profile is established if the value of the director angle on the surface $\theta(1)$ is larger than zero but smaller than $\pi/2$. For the smooth surface the smectic elastic distortions are confined to the narrow region around the cylinder axis. In a very weak anchoring regime, where $\theta(\rho=1)\approx 0$, the undistorted BKS structure is established. Note that these two structures can also be realized for the case of tangential anchoring [20]: e.g., the BKS structure in the case of a smooth surface and the CHV structure if the surface imposes periodicity larger than $d_0=2\pi/q_0$.

It has to be stressed that the ''weak anchoring regime'' of the nematic phase (usually characterized by a strong deviation of the director orientation on the surface from the surface enforced direction) can be substantially shifted towards higher anchoring strengths in the smectic phase. We demon-

strated on a simple case of the distorted BKS structure that the presence of smectic layers in general strongly affects the orientation of nematic molecules at the surface.

Our results are in qualitative accordance with recent experimental results. They can also be applied to the supramicrometer regime where a narrow smectic or nematic melted region is often hard to observe experimentally. The SER structure was observed in the 8CB LC confined to 0.2 $\mu$m diam cylindrical pores of Anopore membranes by Innacchione and Finotello [14] using a high resolution calorimetric study. In the case where the surface was treated with the lecithin they probably observed the CHV or BKS structure. Because of surface irregularities these authors claim that in the lecithin treated sample the surface is wetted with the nematic phase. They observed that the structure with more distorted nematic director field exhibits smaller temperature shift $\Delta T_{NA}$ in the $N-$Sm-$A$ transition temperature in accordance with our calculations. Our analyses indicate that very distorted structure in the nematic director field does not in general cause strong smectic elastic distortions. For example, the smectic-planar-radial structure, which is highly energetic in the nematic free energy contribution, exhibits negligible smectic distortions concomitant with the negligible $N-$Sm-$A$ transition shift $\Delta T_{NA}$.

In the x-ray study [11] the CHV structure was observed in the Sm-$A$ phase of the 8CB LC confined in the glass capillaries of 25 $\mu$m in diameter. The surface was treated with the lecithin, which provides relatively weak homeotropic anchoring. The results suggest a chevron structure, where Sm-$A$ layers are tilted for $\approx 1°$. In the same confining matrix but with different LC (ZLI-3041 and CBC liquid crystal which exhibit in addition to the Sm-$A$ phase also a ferroelectric Sm-$C^*$ phase) Mang, Sakamoto, and Kumar [11] observed a planar nematic director field pattern corresponding to the SPR structure. However, our study indicates that this structure is very unlikely deep in the Sm-$A$ phase because of its energetically expensive nematic deformation. The SER pattern seems to be advantageous. Possible reasons for the stability of the SPR structure deep in the Sm-$A$ phase are pronounced smectic fluctuations in the melted central region of the SER structure. In our approach smectic fluctuations in melted regions reflect in an anomalously increased nematic bend elastic constant $K_{33}$. We showed that with increased $K_{33}$ the melted region progressively shrinks and the SER director profile approaches the SPR one. Above some critical value [6] of the $K_{33}$ constant the escaped-radial director profile can even transform to the radial one [6]. Yet another possibility is that in such large cylinders the relative volume of the melted region of the SER structure, where the director field gradually reorients from the radial direction along the cylinder axis, is negligible. This could cause the SER and SPR structures to be experimentally indistinguishable.

The hybrid hbr structure was probably observed by Crawford *et al.* [13]. They studied 8CB confined in cylindrical capillarities of Nuclepore filters of radius $R \approx 0.1$ $\mu$m using the deuterium NMR. The nontreated Nuclepore surface enforces relatively strong homeotropic anchoring. We could reproduce the shape of their observed absorption spectrum only with the HBR structure with $\rho_c \approx 0.6$ and $\theta_{\mathrm{CHV}} \approx \pi/3$. But our numerical study suggests that the stability of such a structure is questionable. Evidently a more detailed experimental and theoretical analysis is needed for a quantitative description of this structure.

## ACKNOWLEDGMENT

We would like to thank T. J. Sluckin for stimulating discussions and comments.

[1] P. Sheng, Phys. Rev. Lett. **37**, 1059 (1976); Phys. Rev. A **26**, 1610 (1982).
[2] A. Poniewierski and T. J. Sluckin, Liq. Cryst. **2**, 281 (1987).
[3] S. Kralj, S. Žumer, and D. W. Allender, Phys. Rev. A **34**, 2943 (1991).
[4] H. S. Kitzerov, Liq. Cryst. **16**, 1 (1994).
[5] D. W. Allender, G. P. Crawford, and J. W. Doane, Phys. Rev. Lett. **67**, 1442 (1991); G. P. Crawford, D. W. Allender, and J. W. Doane, Phys. Rev. A **45**, 8693 (1992).
[6] S. Kralj and S. Žumer, Phys. Rev. E **51**, 366 (1995).
[7] R. J. O. Crawford, M. Ambrožič, J. W. Doane, and S. Žumer, Phys. Rev. E **50**, 4773 (1994).
[8] *Liquid Crystals in Complex Geometries Formed by Polymer and Porous Networks*, edited by G. P. Crawford and S. Žumer (Taylor and Francis, London, 1995).
[9] P. G. de Gennes and J. Prost, *The Physics of Liquid Crystals* (Oxford University Press, Oxford, 1993).
[10] P. E. Cladis, Philos. Mag. **29**, 641 (1974).
[11] J. T. Mang, K. Sakamoto, and S. Kumar, Mol. Cryst. Liq. Cryst. **223**, 133 (1992).
[12] R. O. Crawford, G. P. Crawford, J. W. Doane, S. Žumer, M. Vilfan, and I. Vilfan, Phys. Rev. E **48**, 1998 (1993).
[13] R. O. Crawford, G. P. Crawford, M. Vilfan, S. Žumer, and J. W. Doane (unpublished).
[14] G. S. Iannacchione and D. Finotello, Phys. Rev. E **50**, 4780 (1994).
[15] N. A. Clark, T. Bellini, R. M. Malzbender, B. N. Thomas, A. G. Rappaport, C. D. Muzny, D. W. Schaefer, and L. Hrubesh, Phys. Rev. Lett. **71**, 3505 (1993).
[16] A. Linhananta and D. E. Sullivan, Phys. Rev. A **44**, 8189 (1991).
[17] M. Kléman, J. Phys. (Paris) **35**, 595 (1974).
[18] P. G. de Gennes, Solid State Commun. **10**, 753 (1972).
[19] S. R. Renn and T. C. Lubensky, Phys. Rev. A **38**, 2132 (1988).
[20] S. Kralj and T. J. Sluckin, Phys. Rev. E **49**, R3244 (1993); **50**, 2940 (1994).
[21] E. B. Priestley, P. J. Wojtowitz, and P. Sheng, *Introduction to Liquid Crystals* (Plenum, New York, 1974), p. 143.
[22] J. Nehring and A. Saupe, J. Chem. Phys. **54**, 337 (1971); **56**, 5527 (1972).
[23] A. Rapini and M. Papoular, J. Phys. (Paris) Colloq. **30**, C4-54 (1969).
[24] G. Vertogen and W. H. de Jeu, *Thermotropic Liquid Crystals* (Springer-Verlag, Berlin, 1988).
[25] I. Vilfan, M. Vilfan, and S. Žumer, Phys. Rev. A **43**, 6875 (1991).
[26] L. Moreau, P. Richetti, and P. Barois, Phys. Rev. Lett. **73**, 3556 (1994).
[27] G. Duran, Liq. Cryst. **14**, 159 (1993).